

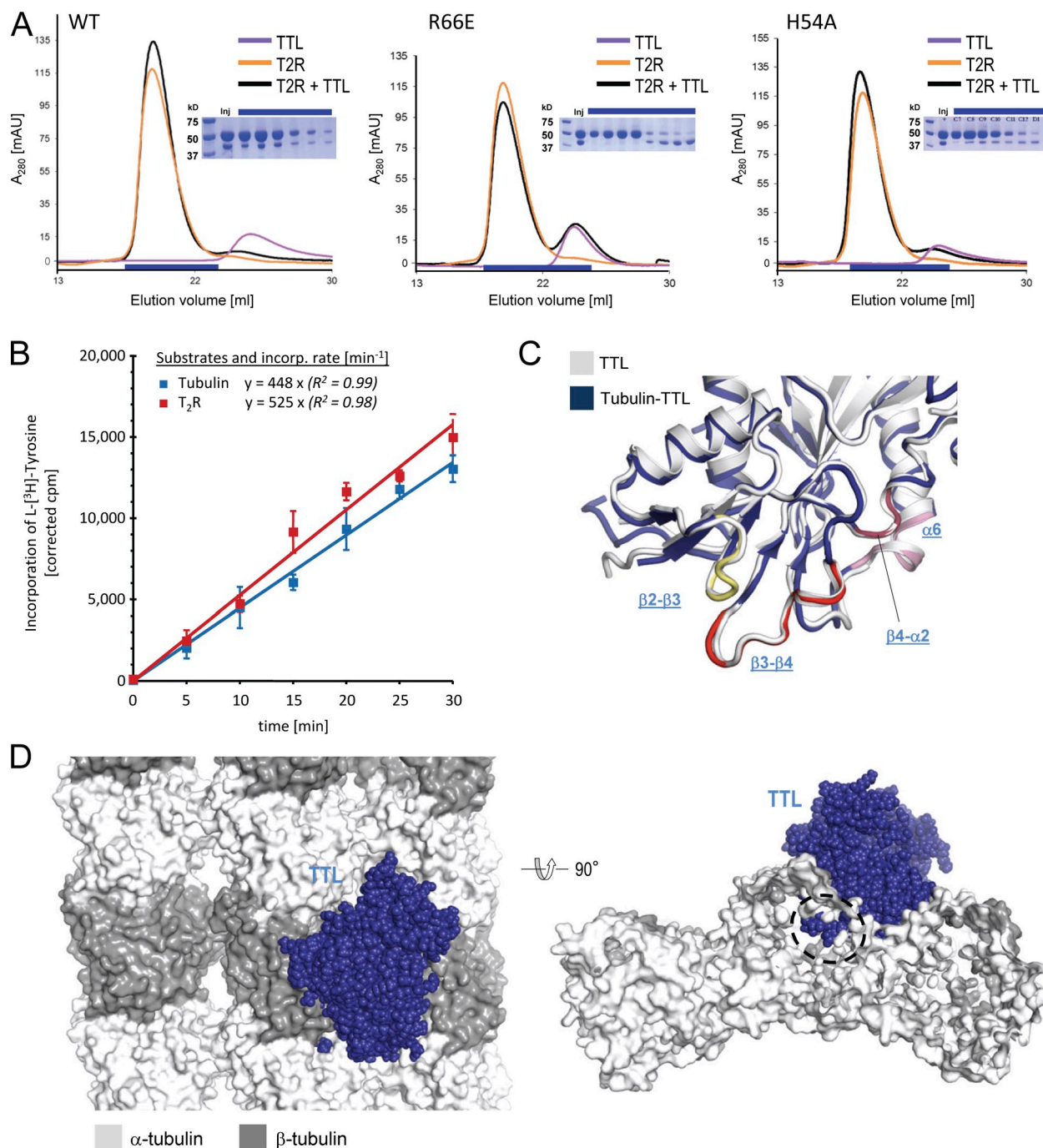
Prota et al., <http://www.jcb.org/cgi/content/full/jcb.201211017/DC1>

Figure S1. **T_2R binding, tyrosination assay, and structural considerations of the TTL-tubulin interaction.** (A) Size exclusion chromatography profiles of T_2R , TTL, and equimolar mixtures of T_2R and TTL. The TTL variants used are indicated on the top left corner of the chromatograms. Insets, SDS-PAGE of the fractions highlighted by a blue bar below the chromatograms. Inj., Sample that was applied onto the size exclusion column. (B) Tyrosination rate of TTL with free tubulin (blue series) or T_2R complex (red series) as substrates. Single measurements of four independent series of experiments were corrected to the incorporation rates of each series. Mean values of the corrected values were plotted and linearly fitted. (C) Close-up view of the superimposition of tubulin-bound (T_2R -TTL, blue) and free TTL (Protein Data Bank accession no. 3TII, gray) in cartoon representation. The three tubulin-interacting TTL loops $\beta 2-\beta 3$, $\beta 3-\beta 4$, and $\beta 4-\alpha 2$, and the N-terminal part of helix $\alpha 6$ are highlighted in pale yellow, red, raspberry, and pink, respectively. (D) Two different views of the TTL-tubulin interaction in the context of the microtubule lattice. The tubulin-TTL structure was extracted from the T_2R -TTL complex (Fig. 1 B) and was superimposed onto a piece of a microtubule (Protein Data Bank accession no. 2XRP; Fourniol et al., 2010). The dashed circle in the left panel highlights the site at the lateral protofilament interface in which TTL (loops $\beta 9-\beta 10$ and $\alpha 7-\beta 14$, helices $\alpha 6$ and $\alpha 7$, and β sheet $\beta 14$) clashes in the microtubule model. α -Tubulin (light gray) and β -tubulin (dark gray) are shown in surface representation; TTL (blue) in sphere representation.

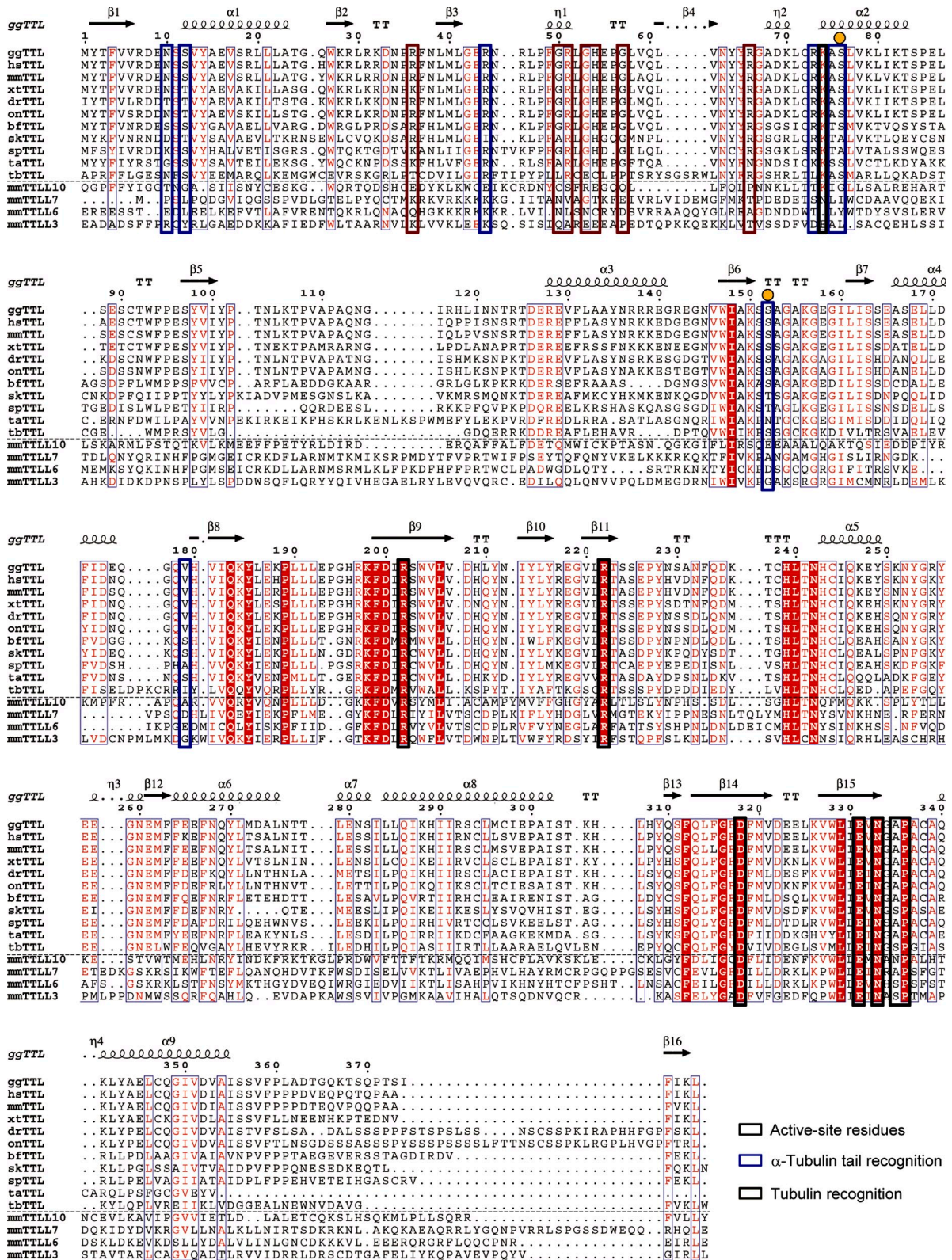


Figure S2. Multiple sequence alignment of TTL orthologues together with selected TTLLs. Structure-based sequence alignment of TTL orthologues with two representative polyglutamylases, mmTTLL4 (initiating enzyme) and mmTTLL6 (elongating enzyme), as well as two polyglycolases, mmTTLL3 (initiating enzyme) and mmTTLL10 (elongating enzyme). The flanking regions of TTLLs are omitted. TTL residues critical for tubulin binding are boxed in green; putative phosphorylation sites are highlighted by an orange closed circle. UniProtKB/Swiss-Prot sequence/NCBI accession numbers are as follows: *Branchiostoma floridae* (*bf*): XP_002610638; *Danio rerio* (*dr*): HF565571; *Gallus gallus* (*gg*): NP_001186321; *Homo sapiens* (*hs*): Q8NG68; *Mus musculus* (*mm*): P38585; *Oreochromis niloticus* (*on*): XP_003441127; *Saccoglossus kowalevskii* (*sk*): XP_002741763; *Strongylocentrotus purpuratus* (*sp*): XP_787911; *Trichoplax adhaerens* (*ta*): XP_002108351; *Trypanosoma brucei* (*tb*): FN554965; *Xenopus tropicalis* (*xt*): AAI57257; mmTTLL6: CAM84326; mmTTLL7: CAM84328; mmTTLL3: CAM84323; mmTTLL10: CAM84331. Active site residues, residues recognizing the α -tubulin tail or the tubulin main body, are highlighted by black, blue, and green boxes, respectively.

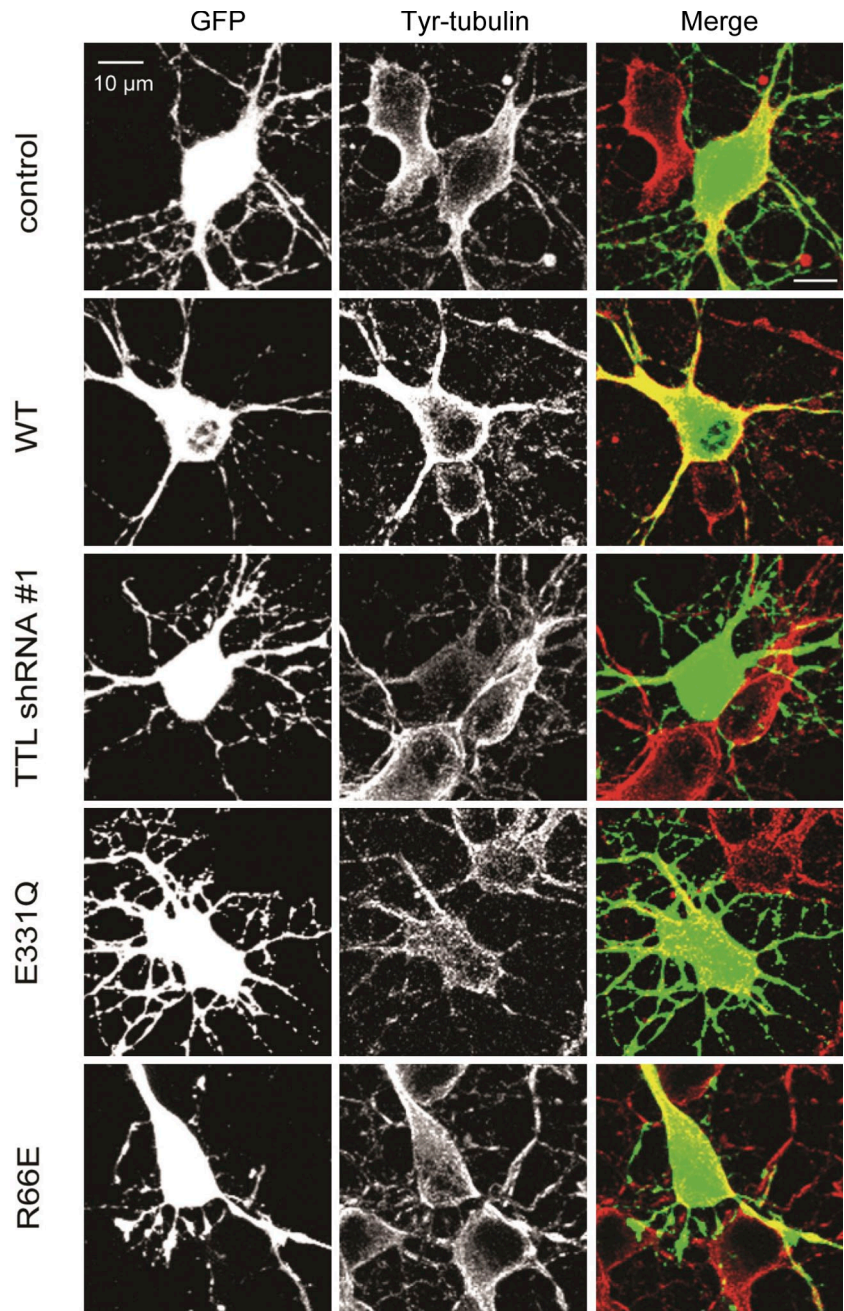


Figure S3. **TTL controls levels of tyrosinated tubulin in cultured hippocampal neurons.** Representative images of hippocampal neurons (DIV5) cotransfected with GFP control, TTL shRNA, wild-type (WT), or mutant forms of TTL, and stained for tyrosinated tubulin. Bar, 10 μ m.

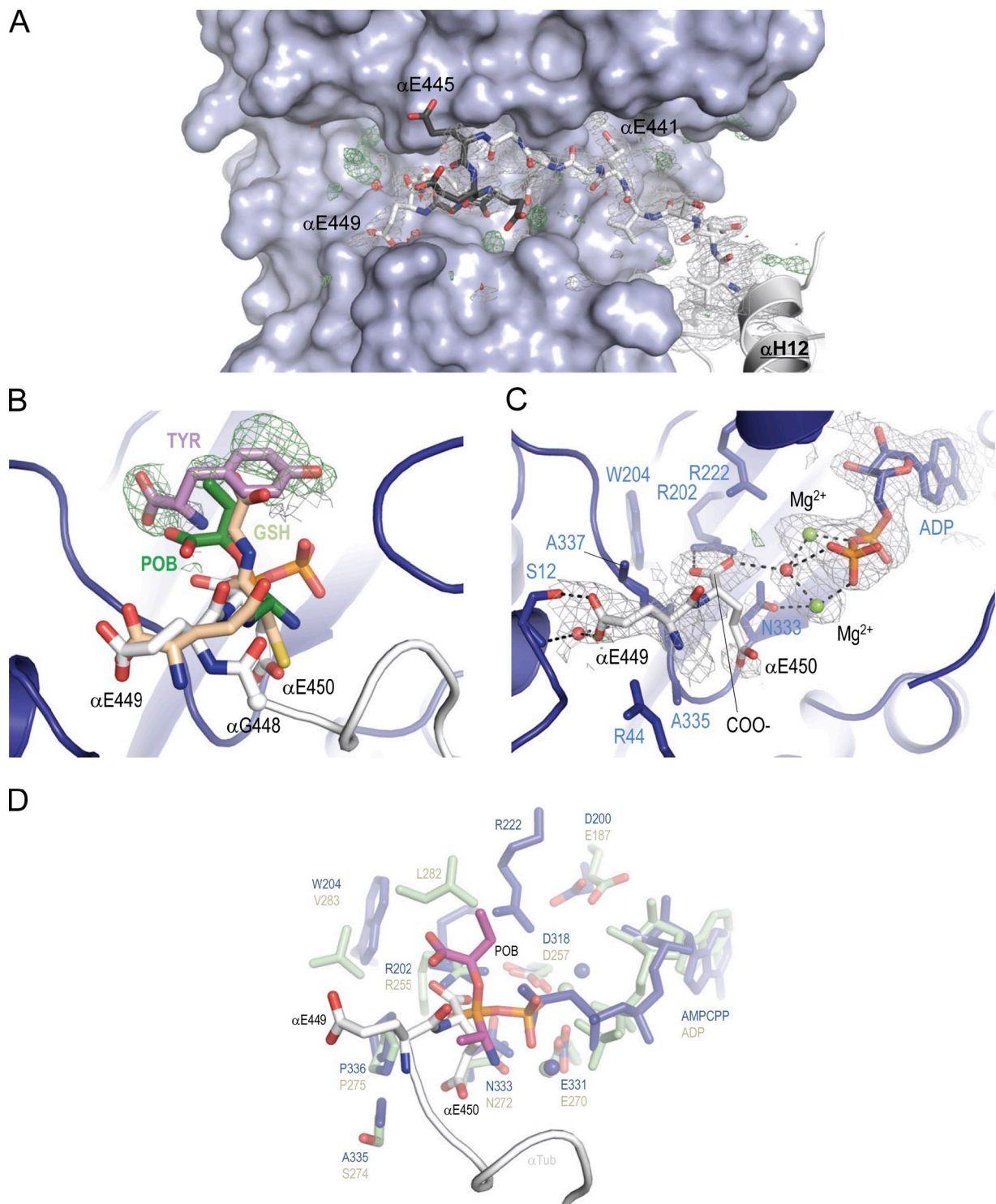


Figure S4. **Electron density of T₂R-TTL structural elements and comparison with ATP-grasp family enzymes.** (A) The 2mFo-DFc (gray mesh) and mFo-DFc (green and red mesh) electron density maps are contoured at 0.7 σ and \pm 3.0 σ , respectively. The α -tubulin tail is in gray sticks, the TTL is in light blue surface representation. Helix α H12 of α -tubulin is shown in light gray cartoon representation. Note that α Glu445, α Glu446, and α Glu447 are not well defined in the electron density and are thus modeled and shown in dark gray. (B) Electron density (mesh) of the putative tyrosine binding pocket in the active site of TTL. The same contour levels as in A are applied. TTL secondary structure elements (cartoon) are depicted in blue and α -tubulin residues (sticks) in gray. A tyrosine molecule is placed in the difference electron density above the main chain carboxylate group of α Glu450 of the α -tubulin tail. The amine group is in favorable orientation to perform the nucleophilic attack for the tyrosination reaction. Note that the tyrosine occupies the same space as the terminal glycine and alanine moieties of the glutathione synthase (light orange; Protein Data Bank accession no. 1GSA) and D-Ala:D-Ala-ligase (dark green; Protein Data Bank accession no. 1IOV) products. (C) Electron density in the active site of TTL bound to ADP. The same contour levels as in A are applied. Both the terminal glutamate moieties (α Glu449 and α Glu450) are shown in stick representation. (D) Superimposition of the active site of TTL (blue) bound to the α -tubulin tail (white) and AMPPCP onto the one of D-Ala:D-Ala ligase (light green; Protein Data Bank accession no. 1IOV) bound to ADP and 2-[[1-amino-ethyl]-phosphate-phosphinoyloxy]-butyric acid (POB; dark gray). For simplicity, only key residue side chains are shown in stick representation. Spheres represent magnesium ions. See Fig. 2 for additional information on labels, symbols, and color code.

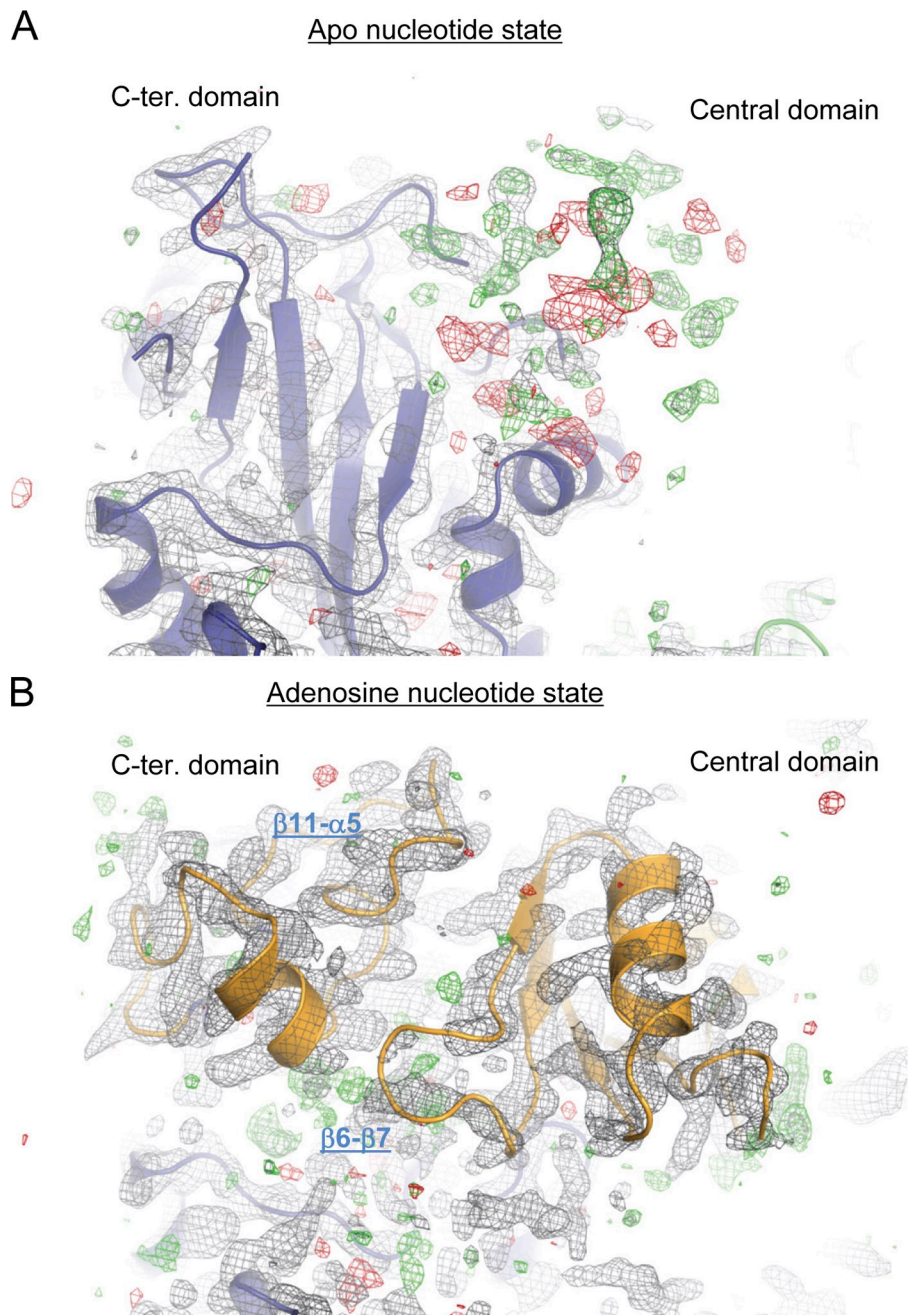


Figure S5. **TTL conformational changes upon tubulin and adenosine nucleotide binding.** Structure of T₂R-TTL obtained in the absence (A) and presence (B) of AMPPCP. TTL is shown in blue cartoon representation with overlaid electron density (mesh). The β 11- α 5 loop and the segment of the central domain that get structured in the presence of tubulin and nucleotide are highlighted in yellow. The 2mFo-DFc (gray mesh) and mFo-DFc (green and red mesh) electron density maps are contoured at 0.9σ and $\pm 3.0\sigma$, respectively.

Table S1. Data collection and refinement statistics

Data collection ^a	T ₂ R-TTL-AMPPCP ^d	T ₂ R-TTL-apo	T ₂ R-TTL-ADP
Space group	P2 ₁ 2 ₁ 2 ₁	P2 ₁ 2 ₁ 2 ₁	P2 ₁ 2 ₁ 2 ₁
Cell dimensions			
a, b, c (Å)	104.8, 158.6, 179.2	103.5, 155.9, 181.0	104.5, 157.3, 181.0
Resolution (Å)	79.4–1.80 (1.85–1.80)	62.3–2.6 (2.67–2.6)	72.1–2.0 (2.05–2.0)
R _{meas} (%)	10.7 (256.5)	17.7 (387.7)	20.0 (316.5)
R _{pim} (%)	3.1 (74.6)	3.8 (88.0)	5.0 (62.9)
CC _{half} ^b	99.9 (36.2)	99.9 (53.5)	99.9 (32.2)
σI	13.4 (1.0)	23.5 (1.1)	13.3 (1.2)
Completeness (%)	99.8 (99.0)	100 (99.9)	99.1 (92.5)
Redundancy	13.5 (13.1)	26.7 (25.7)	26.8 (25.2)
Refinement			
Resolution (Å)	79.4–1.80	62.3–2.6	72.1–2.0
No. unique reflections	274,515 (13,945 in test set)	9,058 (4,511 in test set)	198,893 (10,028 in test set)
R _{work} /R _{free} (%)	17.2/20.5	19.7/23.5	16.8/21.7
Average B-factors (Å²)			
Complex	44.1	67.6	50.3
Solvent	48.1	49.6	52.1
MSA (chain D)	40.0	–	–
Root mean square deviation from ideality			
Bond length (Å)	0.008	0.004	0.008
Bond angles (°)	1.100	0.805	1.140
Ramachandran statistics^c			
Favored regions (%)	98.3	97.1	97.5
Allowed regions (%)	1.6	2.8	2.5
Outliers (%)	0.1	0.1	0

^aHighest shell statistics are in parentheses.

^bAs defined by Karplus and Diederichs (2012).

^cAs defined by MolProbity (Davis et al., 2004).

^dData from Protá et al. (2013).

References

- Davis, I.W., L.W. Murray, J.S. Richardson, and D.C. Richardson. 2004. MOLPROBITY: structure validation and all-atom contact analysis for nucleic acids and their complexes. *Nucleic Acids Res.* 32(Web Server issue):W615–W619. <http://dx.doi.org/10.1093/nar/gkh398>
- Fourniol, F.J., C.V. Sindelar, B. Amigues, D.K. Clare, G. Thomas, M. Perderiset, F. Francis, A. Houdusse, and C.A. Moores. 2010. Template-free 13-protofilament microtubule-MAP assembly visualized at 8 Å resolution. *J. Cell Biol.* 191:463–470. <http://dx.doi.org/10.1083/jcb.201007081>
- Karplus, P.A., and K. Diederichs. 2012. Linking crystallographic model and data quality. *Science.* 336:1030–1033. <http://dx.doi.org/10.1126/science.1218231>
- Protá, A.E., K. Bargsten, D. Zurwerra, J.J. Field, J.F. Diaz, K.-H. Altmann, and M.O. Steinmetz. 2013. Molecular mechanism of action of microtubule-stabilizing anticancer agents. *Science.* <http://dx.doi.org/10.1126/science.1230582>